

Hydrophobicity and Phase Changes of Pd/SiO₂ Organic-inorganic Hybrid Materials Calcined in Air Atmosphere

Jing Yang*, Baosong Li, Hao Xu, Yue Li, Xiang Huo

*School of Environmental & Chemical Engineering, Xi'an Polytechnic University
Xi'an 710048, China*

Abstract

Pd/SiO₂ organic-inorganic hybrid material was prepared by sol-gel method, in which PdCl₂ was added into methyl-modified silica sol. The Pd/SiO₂ sol particle size distribution, the hydrophobicity and phase changes of Pd/SiO₂ hybrid materials calcined at 200, 350, 500, 600 and 750 °C in air atmosphere were discussed. The Pd/SiO₂ sol system exhibits moderate dispersion and the mean particle size of Pd/SiO₂ sol is 2.70 nm. When the calcination temperature is raised to 350 °C, metallic palladium of high crystallinity is formed in the Pd/SiO₂ sample. PdO occurs in minor quantities in the Pd/SiO₂ sample calcined at 500 °C, which increases in amount in the samples calcined at 600 and 750 °C. With the increase of calcination temperature, the Si-CH₃ and Si-OH bands in Pd/SiO₂ materials are found to decrease in absorption intensity and the hydrophobicity on Pd/SiO₂ film surfaces increases. The water contact angle on the Pd/SiO₂ film surface achieves the maximum value as the calcination temperature is up to 350 °C and the particle sizes of the formed metallic Pd are about 15~20 nm. The optimal calcination temperature for hydrophobic Pd/SiO₂ membrane materials is about 350 °C.

Keywords: Sol-gel Method; Palladium Doping; Hydrophobicity; Phase Change

1 Introduction

With the excessive use of carbon based fossil fuels, the world is now facing several great challenges, such as poor air quality, greenhouse gas emissions and high energy consumption rate. Nowadays, it is generally acknowledged that hydrogen would become an environmentally benign alternative to the conventional fossil fuels [1, 2]. However, hydrogen does not exist naturally and has to be produced from hydrogen-containing compounds [3]. Current methods for H₂ separation are solvent adsorption, pressure swing adsorption, cryogenic distillation and membrane separation. Compared with other methods, membrane separation technologies have sufficient selectivity, high permeation flux, minimized unit operations and economic potential in reducing operating costs

*Corresponding author.

Email address: jingy76@163.com (Jing Yang).

[4, 5]. For these reasons, the development for effective hydrogen membranes has engendered considerable interest in academia and industry.

Intensive researches have been conducted on the development of hydrogen separation membranes, including Pd and Pd-alloy membranes, zeolite membranes, carbon molecular sieve membranes, and silica membranes [1, 2, 6]. Pd and Pd-alloy membranes possess ideal H₂ permselectivity from mixed gas streams but suffer from high cost and rapid performance degradation when they get in touch with CO or H₂S [2, 7, 8]. Carbon molecular sieve membranes have excellent H₂ separation properties. However, they are very brittle and fragile and difficult to be prepared as thin supported membranes [6, 9]. Zeolite membranes possess great hydrothermal stability and chemical resistance but show low H₂/CO₂ selectivity, because of the existence of intercrystalline micro defects and the relatively large zeolitic pores [6]. Nowadays other non-Pd-alloy membrane materials, such as Ti-Ni-V, Nb-Ti-Ni, Ni-Nb-Ta and Ta-Ti-Ni alloys, etc., have been investigated by many research groups [7, 10, 11]. However the drawbacks of the alloy membranes are the poor H₂ permeability and the sensibility of hydrogen embrittlement [10]. The maximum hydrogen permeability of the Ni₆₀Nb₃₀Ta₁₀ alloy membrane was 4.13×10^{-8} mol/m·s·Pa^{1/2} at 673 K [10]. Silica membranes tend to be cheaper and economically more attractive. There has been much advancement in controlling the structural formation of microporous silica membranes to deliver high-purity H₂ separation applications [1, 12, 13]. Amorphous silica membranes can be prepared by sol-gel and Chemical Vapour Deposition (CVD) methods [1, 14]. The methods generally show a trade-off in terms of permeability and selectivity. It is well known that silica materials are instable after prolonged exposure to water vapor, which will result in pore blocking and reduced gas permeability [15]. A tremendous amount of work has been done to improve the hydrothermal stability of silica membrane materials, including incorporation of hydrophobic groups [16], heat treatment [17] and introducing some inorganic oxides such as Al₂O₃, MgO, ZrO₂, Co₃O₄, NiO, and Nb₂O₅ [18-23]. From the reports published in the literature [16-23], it has been known that an increase in selectivity is commonly at the expense of a decrease in membrane permeation. Kanezashi *et al.* reported that the Ni-doped silica membranes (Si/Ni=2/1) showed a permeance of 11.2×10^{-7} mol·m⁻²·Pa⁻¹·s⁻¹ for He and 4.5×10^{-8} mol·m⁻²·Pa⁻¹·s⁻¹ for H₂ with a high selectivity of 950 (He/N₂) and 370 (H₂/N₂) when operated at 500 °C and 90 kPa.

Based on the material functional superposition effect, we put forward a new membrane material preparation method, including hydrophobic modification and metallic palladium doping. In this work, Pd/SiO₂ organic-inorganic hybrid material was prepared by sol-gel method, in which PdCl₂ was added into methyl-modified silica sol. The influence of calcining temperature on the hydrophobicity and phase changes of Pd/SiO₂ hybrid material in air atmosphere were investigated by X-ray Diffraction (XRD), fourier transform infrared spectroscopy (FTIR), Thermogravimetric-differential thermogravimetric (TG-DTG) analysis, contact angle and Scanning Electron Microscopy (SEM) measurements. The contact angle measurements were used to quantify the degree of hydrophobicity of Pd/SiO₂ materials.

2 Experimental

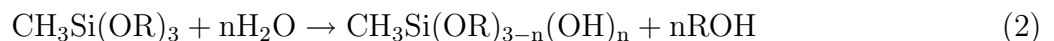
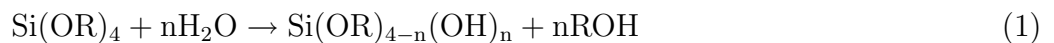
2.1 Pd/SiO₂ Sol Preparation

The Pd/SiO₂ sol was prepared using tetraethylorthosilicate (TEOS, p.a. grade), methyltriethoxysilane (MTES, grade 98%), absolute ethanol (EtOH, grade 99.9%), hydrochloric acid (HCl,

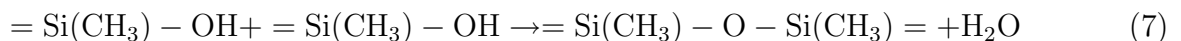
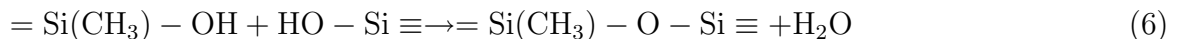
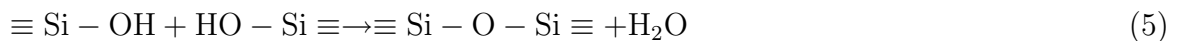
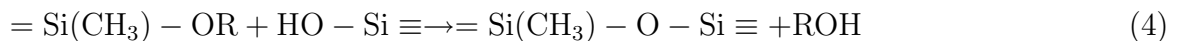
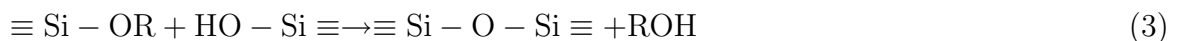
p.a. grade), N, N-dimethyl formamide (DMF, p.a. grade), PdCl₂ (p.a. grade) and deionized water. According to the molar ratio of TEOS/MTES/EtOH/H₂O/HCl=1/0.8/7.6/7.2/0.085, TEOS and MTES were mixed with absolute ethanol in an ice bath. A mixture of HCl and water was slowly added with a dropping funnel to the mixture of TEOS/MTES/EtOH under vigorous stirring. Afterwards the reaction mixture was stirred with water reflux for 3 h at 60 °C. 30% (v/v) DMF was added into the above solution and stirred for 40 min at 25 °C. According to the PdCl₂/TEOS molar ratio of 0.15, 0.1M PdCl₂ solution was added to the mixed sol. After stirring for 40 min, the final solution of ‘Pd/SiO₂’ sol was obtained.

The co-hydrolysis and condensation reactions of TEOS and MTES are as follows [24, 25]:

Hydrolysis reactions:



Condensation reactions:



2.2 Pd/SiO₂ Material Preparation

Unsupported Pd/SiO₂ materials were prepared by pouring sols into Petri dishes and drying the mixture at room temperature. Dried flakes of the formed xerogels were calcined at 200, 350, 500, 600 and 750 °C for 2 h in air atmosphere, respectively. The calcinations are performed using a program controlled high temperature furnace (SLG1100-80 tube furnace, Shanghai, China). The heating rate was 0.5 °C/min and the cooling rate was 1 °C/min. To produce supported Pd/SiO₂ films, dense α-Al₂O₃ supports (of dimensions 20 × 20 × 1.5 mm) were dip-coated into freshly prepared sol and then dried for 3 h at room temperature. After drying, the films were calcined by the same calcination procedure as described above. The coating-drying-calcining process was repeated once more to repair any defects which might be occurred in the first Pd/SiO₂ film layer. Unsupported Pd/SiO₂ materials were made for characterization of XRD, FTIR and TG-DTG and the supported Pd/SiO₂ films were made for characterization of contact angle and SEM measurements.

2.3 Characterization

The particle size measurement of freshly prepared Pd/SiO₂ sol was carried out on a Malvern Nanozs Size Analysis Instrument. The phase structures of Pd/SiO₂ materials were determined by a Rigaku D/max2200pc X-ray diffractometer. FTIR measurements were performed by a Nicolet 5700 spectrometer. TG-DTG analysis was performed by a TGA/SDTA851e with a heating rate of 9 °C/min in air atmosphere. Contact angle measurements were carried out on a JY-82 contact angle analyzer (Chengde, China) to quantify the degree of hydrophobicity. The contact

angles were measured ten times for every sample and the mean value was taken. The surface morphology of the silica membranes were imaged using a JSM-6700F field emission scanning electron microscope with a resolution of 1.0 nm and maximum magnification of 650, 000.

3 Results and Discussion

3.1 Sol Particle Size Analysis

Fig. 1 shows that the hydrodynamic diameter of silica particles in the freshly prepared Pd/SiO₂ sol. As shown in Fig. 1, the sol particle size distribution is relatively narrow and most of the particle diameters are in the range of 2-5.5 nm. The mean particle size of Pd/SiO₂ sol is 2.70 nm. The Particle Dispersion Index (PDI) is 0.438, which means that the sol system exhibits moderate dispersion.

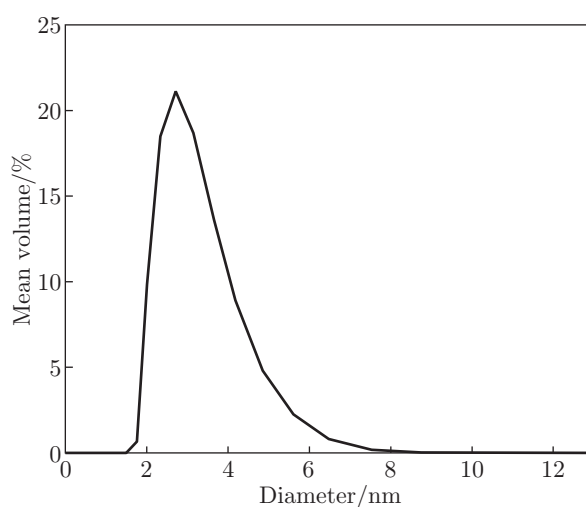


Fig. 1: Particle size distribution of Pd/SiO₂ sol

3.2 XRD Analysis

Fig. 2 shows the XRD patterns of the as-prepared unsupported Pd/SiO₂ materials calcined at different temperatures. A very broad XRD diffraction peak at about $2\theta = 22.21^\circ$ is observed in all the sample XRD curves, which is attributed to the amorphous silica spheres. The strong diffraction peaks of PdCl₂ appear in the XRD curve of non-calcined Pd/SiO₂ materials besides that of the amorphous silica particles and there is no obvious metallic palladium diffraction peaks. It might be because there is no Pd²⁺ being reduced or the amount of reduced Pd²⁺ is too small to be detected. When the sample is calcined at 200 °C, the diffraction peaks of PdCl₂ decrease greatly and there is still no obvious metallic palladium diffraction peaks appearing. By further increasing the calcination temperature up to 350 °C, the diffraction peaks assigned to the (111), (200), (220), (311) and (222) planes of a Face Centered Cubic (FCC) lattice of Pd at $2\theta = 40.12, 46.66, 68.12, 82.10$ and 86.62° , respectively, can be clearly observed, which indicates the formation of pure palladium of high crystallinity. In the XRD curve of Pd/SiO₂ materials calcined at 350 °C, only the diffraction peaks of the palladium crystals can be observed and those of PdCl₂ disappeared

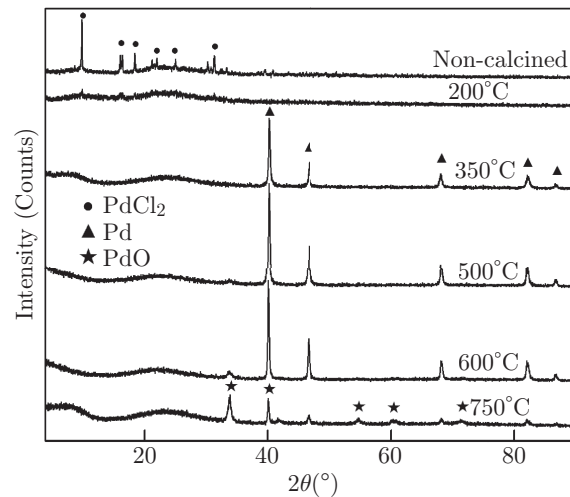
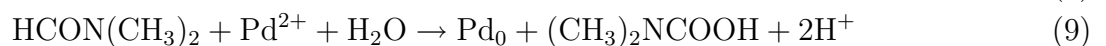
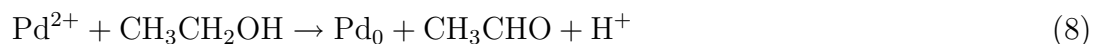


Fig. 2: XRD pattern of Pd/SiO₂ materials calcined at different temperatures

completely. As the calcination temperature is increased to 500 °C, a new weak diffraction peak at about $2\theta = 33.80^\circ$ appears, which enhances for the samples calcined at 600 and 750 °C. It is remarkable that, in the XRD curve of Pd/SiO₂ materials calcined at 750 °C, the diffraction peaks assigned to the (101), (110), (112), (103) and (222) planes of PdO at $2\theta = 33.82, 41.79, 54.76, 60.25$ and 71.30° , respectively, can be clearly observed. At the same time, the diffraction peaks of metallic palladium diminish in intensity. This led to the conclusion that the new diffraction peak at $2\theta = 33.8^\circ$ appearing in the sample curve that calcined at 500 °C is due to crystalline PdO. This means that, when the calcination temperature is increased to 500 °C, a small part of metallic palladium will be converted to PdO. Because the thermal-decomposition temperature of PdCl₂ is 500 °C, the fact that metallic palladium appears in the Pd/SiO₂ materials calcined at 350 °C shows that the formation of metallic palladium results from the reduction of Pd²⁺, not the thermal decomposition of PdCl₂. Ethanol is a weak reductant which can reduce many metallic salts. And at the same time, DMF can also function as reductants besides being used as drying controllers. The following reaction takes place under heat-treatment condition during the process:



The full width at half-maximum of the strongest characteristic reflection (111) was used to estimate the average crystallite size by applying the Scherrer equation [26]:

$$d = 0.9\lambda/(\beta \cos \theta) \quad (11)$$

where d is the mean diameter of the Pd particle, λ is the wavelength of the X-ray source (CuK $\alpha=1.54056\text{\AA}$), and β is the Full-width at Half-maximum (FWHM) of the X-ray diffraction peak at the diffraction angle θ . Hence, the mean Pd diameter estimated in the Pd/SiO₂ materials calcined at 350 °C is about 21.8 nm.

3.3 TG-DTG Analysis

Fig. 3 depicts the TG-DTG curves of non-calcined Pd/SiO₂ materials. In the calcining process, the condensation reactions such as Equations (3)-(7) will continue to occur. In Fig. 3, there are three obvious weight loss peaks in DTG curve, which is located at 58, 238 and 590 °C, respectively. This means that it has passed through three clear weight loss stages in the thermogravimetric analysis process. The sharp weight loss of 4.1% from approximately 30 ~ 120 °C is mainly caused by the evaporation of residual water and ethanol. The great weight decrease between 120 °C and 300 °C is mainly attributed to the decomposition of DMF and Si-OR that doesn't completely react. The weight loss in the 2nd stage is about 36.7% and the weight loss velocity achieves the maximum value at 238 °C. Above 300 °C, the Pd/SiO₂ sample shows a weight loss of 7.3%, due to the condensation dehydration and the decomposition of Si-CH₃ groups.

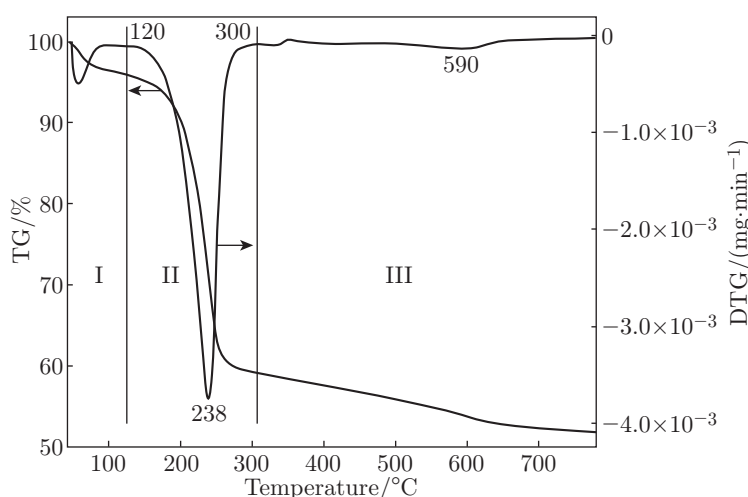


Fig. 3: TG-DTG curves of Pd/SiO₂ materials in air atmosphere

3.4 FTIR Analysis

The FTIR spectra of Pd/SiO₂ materials calcined at different temperatures are depicted in Fig. 4. In Fig. 4, the bands at 1051, 792 and 443 cm⁻¹ are due to the Si-O asymmetric stretching, Si-O symmetric stretching and Si-O-Si bending vibrations, respectively [27-30]. The band at 940 cm⁻¹ is attributed to the O-H stretching vibration in Si-OH group. The bands at 1386, 2925, 2978 cm⁻¹ are associated with the vibration of -CH₃ group and that at 1467 cm⁻¹ is attributed to CH₂ group. The absorption peak at 1276 cm⁻¹ is due to Si-CH₃ group and that at 2780 cm⁻¹ corresponds to C-H band in O=CH group. The absorption peak at 3100 cm⁻¹ corresponds to the combined vibration of N-H and C-N bands in DMF and those at 1640 and 3450 cm⁻¹ are ascribed to O-H groups arising from the adsorption water by Si-OH [31]. From Fig. 4, we can see that the Si-CH₃ absorption peak at 1276 cm⁻¹ and the Si-OH absorption peak at around 940 cm⁻¹ are observed to weaken with the increasing calcining temperature. When the calcining temperature reaches 350 °C, the absorption peaks at 1467, 2780 and 3100 cm⁻¹ disappear, indicating the complete decomposition of Si-OR and DMF. It is noteworthy that, when the calcining temperature arrives 600 °C, the Si-CH₃ band at 1276 cm⁻¹ diminishes greatly in intensity. As the calcining temperature is further increased to 750 °C, it completely disappears, suggesting the further organic-to-inorganic transformation of Si-CH₃ groups.

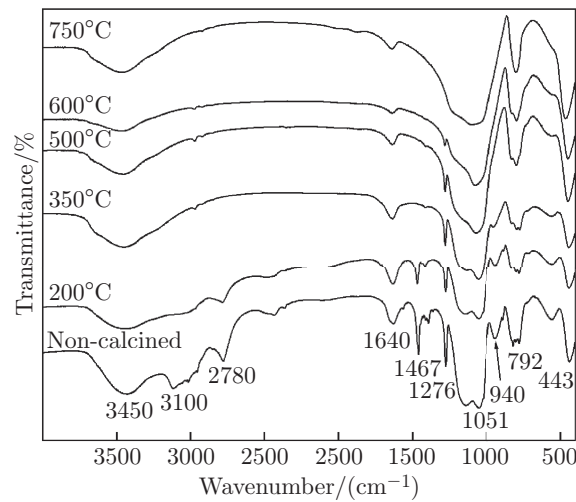
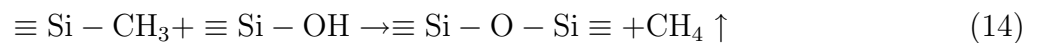
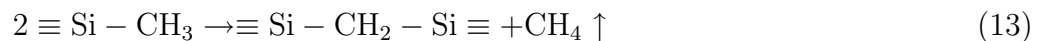
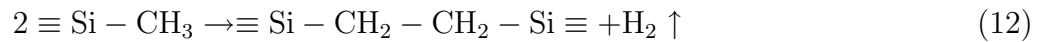
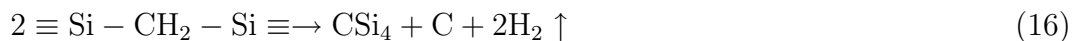
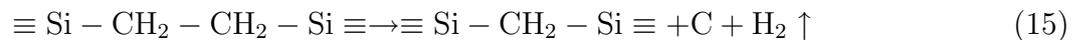


Fig. 4: FTIR spectra of Pd/SiO₂ materials calcined at different temperatures

As the calcining temperature is high enough, the Si-CH₃ groups will begin to decompose, which could be described by Equations (12)-(14):



With the further increase of calcining temperature, the components in Pd/SiO₂ materials will mineralize and the Si-CH₃ band at 1276 cm⁻¹ disappears. The reactions that might occur are as follows:

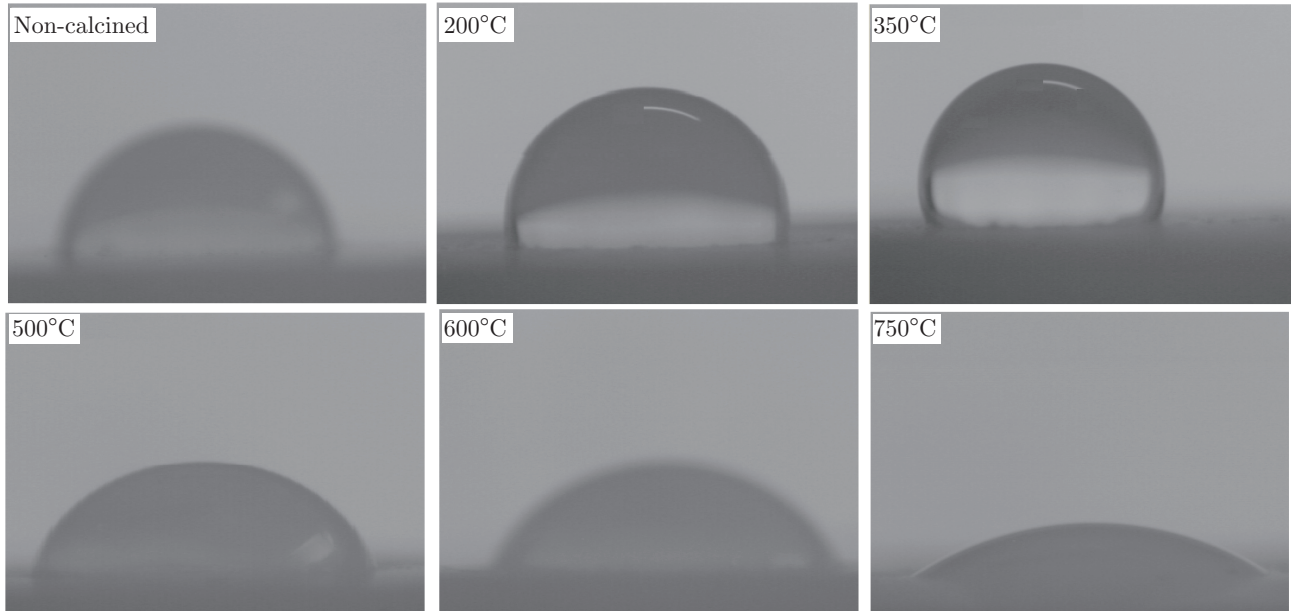


3.5 Variation in Contact Angles

The wetting property of a solid surface is generally characterized by the water contact angle (θ) measurement. It is well known that $\theta < 90^\circ$ and $\theta > 90^\circ$ can indicate surface ‘hydrophilicity’ or ‘hydrophobicity’, respectively [32]. The water contact angles of Pd/SiO₂ films calcined at different temperatures are listed in Table 1. Table 1 shows the water contact angles of Pd/SiO₂ films increase with the increasing calcining temperature while they begin to decrease as the calcining temperature is above 350 °C. The Pd/SiO₂ film surfaces calcined at 200 and 350 °C are hydrophobic. With the progress of calcination, the residual water and ethanol in the Pd/SiO₂ material will be removed. On the other hand, the components in the samples will continue to condense and the number of O-H groups on the Pd/SiO₂ film surfaces will decrease. Hence, the hydrophobicity and water contact angles of Pd/SiO₂ films will increase with the increasing calcining temperature. The sharp decrease in the water contact angle above 350 °C might be because some of the Si-CH₃ groups have been decomposed. This means the decomposition temperature of CH₃ groups is below 500 °C. The water drop images on Pd/SiO₂ film surfaces at various calcinations temperatures are shown in Fig. 5.

Table 1: Water contact angles of Pd/SiO₂ films calcined at various temperature in air atmosphere

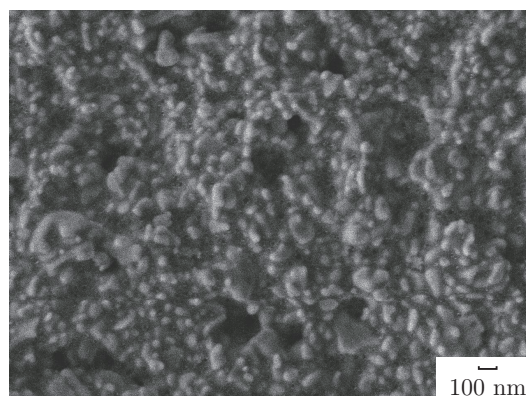
Calcination temperature (°C)	Non-calcined	200	350	500	600	750
Contact angle (°)	90.58±0.61	91.84±0.70	98.56±0.95	63.42±1.16	45.35±1.08	30.30±0.98

Fig. 5: Water drop images on Pd/SiO₂ film surfaces calcined at various temperature in air atmosphere

Thus, according to the XRD, TG-DTG, FTIR and contact angle analysis as described above, in order to keep the hydrophobicity of Pd/SiO₂ membrane materials, the optimal calcination temperature is about 350 °C and the allowable operating temperature for Pd/SiO₂ membranes in oxygenated environment is below 350 °C.

3.6 SEM Image

Fig. 6 shows the surface images for Pd/SiO₂ film calcined at 350 °C. In Fig. 6, the particle distribution on the film surface is a relatively narrow and most of the particle diameters are 4~8

Fig. 6: SEM surface image of Pd/SiO₂ film calcined at 350 °C

nm. A small amount of larger particles were observed which are due to the formed metallic Pd and their particle sizes are about 15~20 nm. It can be seen that the particle size observed from SEM is similar to that calculated from XRD analysis.

4 Conclusion

The particle size distribution of the freshly prepared Pd/SiO₂ sol is relatively narrow and the mean particle size of Pd/SiO₂ sol is 2.70 nm. In the XRD curve of Pd/SiO₂ materials non-calcined and calcined at 200 °C, only the diffraction peaks of PdCl₂ can be observed and there is no obvious metallic palladium diffraction peaks appearing. By further increasing the calcination temperature up to 350 °C, the diffraction peaks of metallic palladium can be clearly observed and those of PdCl₂ disappear completely. However, as the calcination temperature is increased to 500 °C, a new weak diffraction peak assigned to PdO appear, which enhances in intensity for the samples calcined at 600 and 750 °C. FTIR shows the absorption peaks of Si-CH₃ and Si-OH bands in Pd/SiO₂ materials weaken with the increasing calcining temperature. When the calcining temperature is up to 600 °C, the Si-CH₃ band diminishes greatly in intensity, which completely disappears when the calcining temperature arrives 750 °C. The water contact angle on the Pd/SiO₂ film surface achieves the maximum value as the calcination temperature is 350 °C and the particle sizes of the formed metallic Pd are about 15~20 nm. To keep the hydrophobicity of Pd/SiO₂ membrane materials, the optimal calcination temperature is about 350 °C and the allowable operating temperature for Pd/SiO₂ membranes in oxygenated environment is below 350 °C.

Acknowledgement

The authors acknowledge the financial assistance from the National Natural and Science Foundation Council of China 21103132, Natural Science Foundation of Shaanxi Province, China 2011JQ2016, the special item of Shaanxi Educational Committee, China 12JK0591 and the Doctoral Science Foundation of Xi'an Shaanxi Polytechnic University, China BS1006.

References

- [1] Gopalakrishnan S, da Costa JCD. Hydrogen gas mixture separation by CVD silica membrane. *J Membr Sci* 2008; 1: 144-147.
- [2] Qiao A, Zhang K, Tian Y, Xie LL, Luo HJ, Lin YS, Li YD. Hydrogen separation through palladium-copper membranes on porous stainless steel with sol-gel derived ceria as diffusion barrier. *Fuel* 2010; 6: 1274-1279.
- [3] Meng XX, Song J, Yang NT, Meng B, Tan XY, Ma ZF, Li K. Ni-BaCe_{0.95}Tb_{0.05}O_{3-δ} cermet membranes for hydrogen permeation. *J Membr Sci* 2012; 401-402: 300-305.
- [4] Yun S, Oyama ST. Correlations in palladium membranes for hydrogen separation: A review. *J Membr Sci* 2011; 1-2: 28-45.
- [5] Moon JH, Bae JH, Bae YS, Chung JT, Lee CH. Hydrogen separation from reforming gas using organic templating silica/alumina composite membrane. *J Membr Sci* 2008; 1-2: 45-55.

- [6] Li YS, Liang F, Bux H, Yang W, Caro J. Zeolitic imidazolate framework ZIF-7 based molecular sieve membrane for hydrogen separation. *J Memb Sci* 2010; 1-2: 48-54.
- [7] Ahmad AL, Jaya MAT, Derek CJC, Ahmad MA. Synthesis and characterization of TiO₂ membrane with palladium impregnation for hydrogen separation. *J Memb Sci* 2011; 1-2: 166-175.
- [8] Huang TC, Wei MC, Chen HI. Preparation of hydrogen-permselective palladium-silver alloy composite membranes by electroless co-deposition. *Sep Purif Technol* 2003; 1-3: 239-245.
- [9] Ismail AF, David LIB. A review on the latest development of carbon membranes for gas separation. *J Memb Sci* 2001; 1: 1-18.
- [10] Kim KB, Kim KD, Lee DY, Kim YC, Fleury E, Kim DH. Hydrogen permeation properties of Pd-coated Ni₆₀Nb₃₀Ta₁₀ amorphous alloy membrane. *Mater Sci Eng A* 2007; 449-451: 934-936.
- [11] Song G, Dolan MD, Kellam ME, Liang D, Zambelli S. V-Ni-Ti multi-phase alloy membranes for hydrogen purification. *J Alloys Compd* 2011; 38: 9322-9328.
- [12] Lee D, Zhang L, Oyama ST, Niu S, Saraf RF. Synthesis, characterization, and gas permeation properties of a hydrogen permeable silica membrane supported on porous alumina. *J Memb Sci* 2004; 1-2: 117-126.
- [13] Da Costa JCD, Lu GQ, Rudolph V, Lin YS. Novel molecular sieve silica (MSS) membranes: characterisation and permeation of single-step and two step sol-gel membranes. *J Memb Sci* 2002; 1: 9-21.
- [14] Gestel TV, Hauler F, Bram M, Meulenber WA, Buchkremer HP. Synthesis and characterization of hydrogen-selective sol-gel SiO₂ membranes supported on ceramic and stainless steel supports. *Sep Purif Technol* 2014; 121: 20-29.
- [15] Uhlmann D, Smart S, da Costa JCD. High temperature steam investigation of cobalt oxide silica membranes for gas separation. *Sep Purif Technol* 2010; 2: 171-178.
- [16] Wei Q, Li JL, Song CL, Liu W, Chen CS. Preparation, characterization and hydrothermal stability of hydrophobic methyl-modified silica membrane. *J Inorg Mater(China)* 2004; 19: 417-423.
- [17] Vos RM, Maier WF, Verweij H. Hydrophobic silica membranes for gas separation. *J Membr Sci* 1999; 158: 277-288.
- [18] Nam SW, Ha HY, Yoon SP, Han J, Lim TH, Oh IH, Hong SA. Hydrogen-permselective TiO₂/SiO₂ membranes formed by chemical vapor deposition. *J Korean Membr* 2001; 3: 69-74.
- [19] Yoshida K, Hirano Y, Fujii H, Tsuru T, Asaeda M. Hydrothermal stability and performance of silica-zirconia membranes for hydrogen separation in hydrothermal conditions. *J Chem Eng Jpn* 2001; 34: 523-530.
- [20] Uhlmann D, Liu S, Ladewig BP, da Costa JCD. Cobalt-doped silica membranes for gas separation. *J Membr Sci* 2009; 326: 316-321.
- [21] Gu Y, Hacırlıoğlu P, Oyama ST. Hydrothermally stable silica-alumina composite membranes for hydrogen separation. *J Membr Sci* 2008; 310: 28-37.
- [22] Kanezashi M, Asaeda M. Hydrogen permeation characteristics and stability of Ni-doped silica membranes in steam at high temperature. *J Membr Sci* 2006; 271: 86-93.
- [23] Boffa V, Blank DHA, Elshof JET. Hydrothermal stability of microporous silica and niobia-silica membranes. *J Membr Sci* 2008; 319: 256-263.
- [24] Liu RL, Xu Y, Wu D, Sun YH, Gao HC, Yuan HZ, Deng F. Comparative study on the hydrolysis kinetics of substituted ethoxysilanes by liquid-state ²⁹Si NMR. *J Non-Cryst Solids* 2004; 1-3: 61-70.
- [25] Xu Y, Liu RL, Wu D, Sun YH, Gao HC, Yuan HZ, Deng F. Ammonia-catalyzed hydrolysis kinetics of mixture of tetraethoxysilane with methyltriethoxysilane by ²⁹Si NMR. *J Non-Cryst Solids* 2005; 30-32: 2403-2413.

- [26] Ryu JH, Chang DS, Choi BG, Yoon JW, Lim CS, Shim KB. Fabrication of Ag nanoparticles-coated macroporous SiO₂ structure by using polystyrene spheres. *Mater Chem Phys* 2007; 2-3: 486-491.
- [27] Bhagat SD, Kim YH, Ahn YS. Room temperature synthesis of water repellent silica coatings by the dip coat technique. *Appl Surf Sci* 2006; 253: 2217-2221.
- [28] Zhang Z, Tanigami Y, Terai R, Wakabayashi H. Preparation of transparent methyl-modified silica gel. *J Non-Cryst Solids* 1995; 189: 212-217.
- [29] Lee S, Cha YC, Hwang HJ, Moon JW, Han IS. The effect of pH on the physicochemical properties of silica aerogels prepared by an ambient pressure drying method. *Mater Lett* 2007; 61: 3130-3133.
- [30] Jiang HM, Zheng Z, Wang XL. Kinetic study of methyltriethoxysilane (MTES) hydrolysis by FTIR spectroscopy under different temperatures and solvents. *Vib Spectrosc* 2008; 46: 1-7.
- [31] Yang J, Chen JR. Surface free energies and steam stability of methyl-modified silica membranes. *J Porous Mater* 2009; 16: 737-744.
- [32] Nosonovskya M, Bhushan B. Hierarchical roughness optimization for biomimetic superhydrophobic surfaces. *Ultramicroscopy* 2007; 10-11: 969-979.